AGU PUBLICATIONS

Geophysical Research Letters

RESEARCH LETTER
10.1002/2017GL076368

Key Points:
- Transient fluid expulsion causes elevated thermal gradients on the seafloor landward of the pinch out of the base of gas hydrate stability
- Temperatures within the gas hydrate stability field are depressed by endothermic cooling from gas hydrate dissociation
- Double-BSRs in the study area are likely to be caused by uplift from subduction of a seamount, which also causes fluid expulsion

Supporting Information:
- Supporting Information S1
- Table S1
- Table S2

Correspondence to:
I. A. Pecher,
i.pecher@auckland.ac.nz

Citation:
Pecher, I. A., Villinger, H., Kaul, N., Crutchley, G. J., Mountjoy, J. J., Huhn, K., … Coffin, R. B. (2017). A fluid pulse on the Hikurangi subduction margin: Evidence from a heat flux transect across the upper limit of gas hydrate stability. *Geophysical Research Letters*, *44*, 12,385–12,395. https://doi.org/10.1002/2017GL076368

Received 14 JUL 2017
Accepted 10 DEC 2017
Accepted article online 14 DEC 2017
Published online 29 DEC 2017

A Fluid Pulse on the Hikurangi Subduction Margin: Evidence From a Heat Flux Transect Across the Upper Limit of Gas Hydrate Stability

I. A. Pecher[1], H. Villinger[2], N. Kaul[3], G. J. Crutchley[4], J. J. Mountjoy[5], K. Huhn[3], N. Kukowski[6], S. A. Henrys[4], P. S. Rose[7], and R. B. Coffin[7]

[1]School of Environment, University of Auckland, Auckland, New Zealand, [2]Department of Geosciences, University of Bremen, Bremen, Germany, [3]MARUM, University of Bremen, Bremen, Germany, [4]GNS Science, Lower Hutt, Wellington, New Zealand, [5]NIWA, Wellington, New Zealand, [6]University of Jena, Jena, Germany, [7]Texas A&M University Corpus Christi, Corpus Christi, TX, USA

Abstract A transect of seafloor heat probe measurements on the Hikurangi Margin shows a significant increase of thermal gradients upslope of the updip limit of gas hydrate stability at the seafloor. We interpret these anomalously high thermal gradients as evidence for a fluid pulse leading to advective heat flux, while endothermic cooling from gas hydrate dissociation depresses temperatures in the hydrate stability field. Previous studies predict a seamount on the subducting Pacific Plate to cause significant overpressure beneath our study area, which may be the source of the fluid pulse. Double-bottom simulating reflections are present in our study area and likely caused by uplift based on gas hydrate phase boundary considerations, although we cannot exclude a thermogenic origin. We suggest that uplift may be associated with the leading edge of the subducting seamount. Our results provide further evidence for the transient nature of fluid expulsion in subduction zones.

1. Introduction

Changes in subseafloor temperature or pressure can lead to dissociation of solid gas hydrates to water and free gas. This process has long been thought to affect seafloor stability and to play a role in climate change (e.g., Kvenvolden, 1993). A number of studies have focused on gas hydrate dissociation following ocean warming and sea level lowering (e.g., Davy et al., 2010; Goto et al., 2016; Phrampus & Hornbach, 2012) as well as the effects of subsurface fluid flow (e.g., Crutchley et al., 2014; Tréhu et al., 2003).

Dewatering in subduction zones may lead to significant fluid flow resulting in advective transport of heat along with upward migrating fluids (e.g., Kukowski & Pecher, 1999; Saffer & Bekins, 1999). Many studies of advective heat flux in subduction margins implicitly assume steady state, long-term fluid expulsion. Fluid expulsion, however, may be transient (e.g., Saffer & Bekins, 1998). The response of gas hydrates to resulting transient warming will, in particular, be affected by the endothermic nature of hydrate dissociation. We present results from combined analysis of heat flux from the depth of bottom simulating reflections (BSRs) at the base of gas hydrate stability (BGHS) and a seafloor heat flux transect on the Hikurangi Margin east of New Zealand, where the Pacific Plate is being subducted beneath the Australian Plate (Figure 1).

Our study area contains double-BSRs (Pecher et al., 2014) (Figure 2). The deeper of double- or multiple BSRs are often thought to be paleo-BSRs resulting from free gas that remains trapped at the paleo-level of the BGHS before a pressure decrease caused by tectonic uplift (Foucher et al., 2002), an increase of bottom-water temperature (Bangs et al., 2005), or rapid burial following sedimentation pulses (Zander et al., 2017). Alternatively, the deeper BSR may mark the phase boundary of Structure-II (sII) hydrate that forms from gas mixes with higher-order hydrocarbons in addition to methane and is more stable than Structure-I (sI) methane hydrate. Sub-BSR sII hydrates have been recovered in industry wells east of Borneo (Paganoni et al., 2016), although without evidence for a double-BSR.

For our study area, Pecher et al. (2014) established that the shallower BSR, BSR-1, marks the current base of methane gas hydrate stability and ruled out any diagenetic origin of the deeper BSR, BSR-2, based on seismic polarity. Any regional changes, for example, of bottom-water temperatures are unlikely to cause the double-BSR because of convergence of both BSRs toward the southwestern part of our study area (Figure 3). The double-BSR is located beneath a seafloor ridge without any indications for significant recent

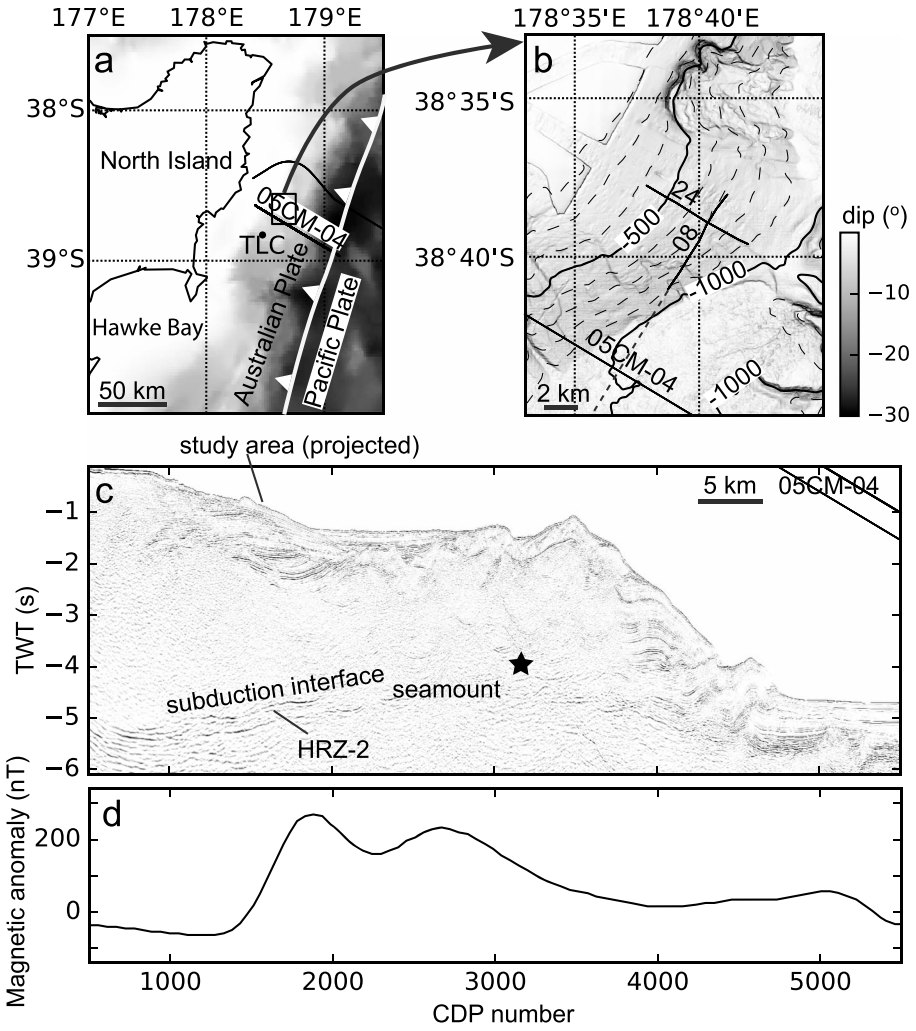

Figure 1. (a) Tectonic setting. TLC: Tuaheni Landslide Complex, referred to in the discussion. (b) Location map. Contour interval 100 m with dip in grey scale. Lines 8 and 24 are analyzed here (solid lines: shown in Figures 2a and 3a; dashed line, continuation of line 8 that extends beyond map, shown in Figure 3c). (c) Deep-penetration seismic profile 05CM-04. HRZ-2 is one of the high reflectivity zones reported by Bell et al. (2010). Star: approximate location of the 1947 Offshore Bay of Plenty earthquake referred to in the discussion (Bell et al., 2014). (d) Magnetic anomaly along line 05CM-04 (Bell et al., 2014; Sutherland, 1996).

sedimentation, making sedimentation pulses an unlikely cause of paleo-BSRs. Two mechanisms for the formation of BSR-2 were proposed (Pecher et al., 2014), admixing of sII-forming gases and a paleo-BSR marking the BGHS before local uplift. We further investigate these possible causes of the double-BSRs.

2. Data and Methods

We analyzed seismic data acquired in 2011 during a high-resolution 2-D survey by the R/V *Tangaroa*, TAN1114, with two 740-1720 cm^3 (45-105 cu-in) generator-injector air guns and a 48-channel streamer with 12.5 m group spacing (Barnes & TAN 1114 Scientific Party, 2011). Data processing included common depth point reflection (CDP) sorting, normal-moveout correction with a velocity of 1,500 m/s, stacking, poststack finite difference time migration, and removal of residual system delays. Streamer length was too short for velocity analysis.

Seafloor heat flux was measured on the R/V *Sonne* during voyage SO-247 (Huhn, 2016) using the University of Bremen's Giant Heat flux Probe, a 6 m long violin bow design comprising 21 thermistors (Hyndman et al., 1979; Villinger et al., 2010). In situ thermal conductivity was determined at six stations using the pulse probe method (Lister, 1979).

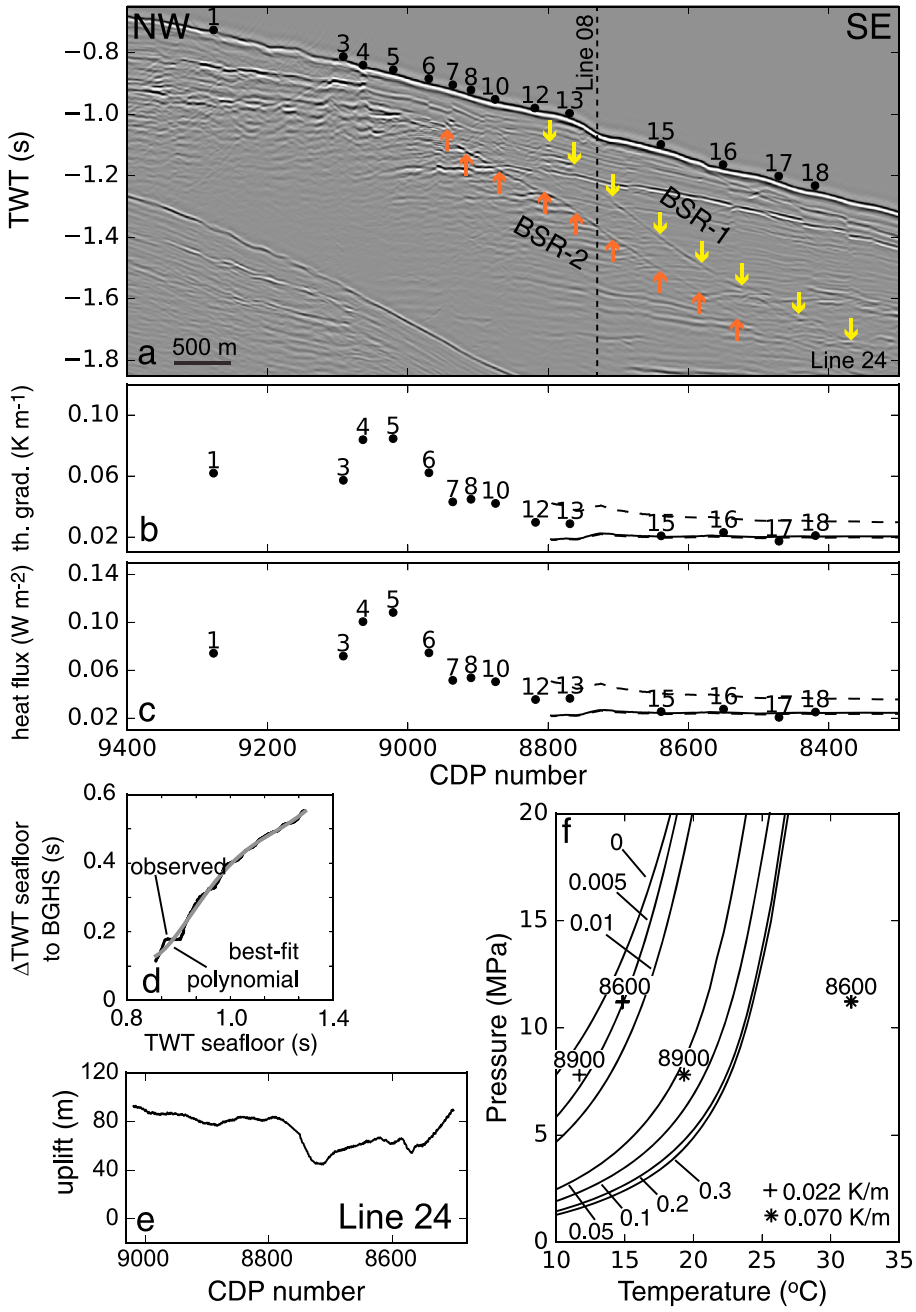

Figure 2. (a) Seismic line 24 with locations of successful deployments of seafloor heat probes. The dashed vertical line marks crossing with line 8 (Figure 3). (b and c) Thermal gradient ("th. grad.") and heat flux, respectively. Dots: from seafloor heat probes. Lines: from BSR-1. Solid line: baseline (hydrostatic pressure, sediment velocity 1,700 m/s, seawater). Dashed lines: upper (lithostatic, velocity 1,600 m/s, freshwater) and lower (hydrostatic, velocity 1,800 m/s, seawater) bounds. (d) TWT difference between BSR and seafloor as a function of TWT to the seafloor along line 24 used to predict uplift. (e) Uplift calculated assuming BSR-2 is paleo-BSR before uplift event. (f) Phase boundary for hydrates from a methane-propane mix in seawater; labels: propane fraction. Predicted pressure-temperature points at the depth of BSR-2 at CDPs 8,600 and 8,900 for background and elevated thermal gradients. Refer to text for further details.

2.1. Seafloor and BSR Thermal Data

Thermal gradients were calculated from temperature-depth profiles from the heat probe data starting at subseafloor depths at which the profiles were sufficiently linear to rule out seasonal bottom-water temperature effects (>1–2 m beneath the seafloor; mbsf; Figure S1 in the supporting information). Temperature gradients

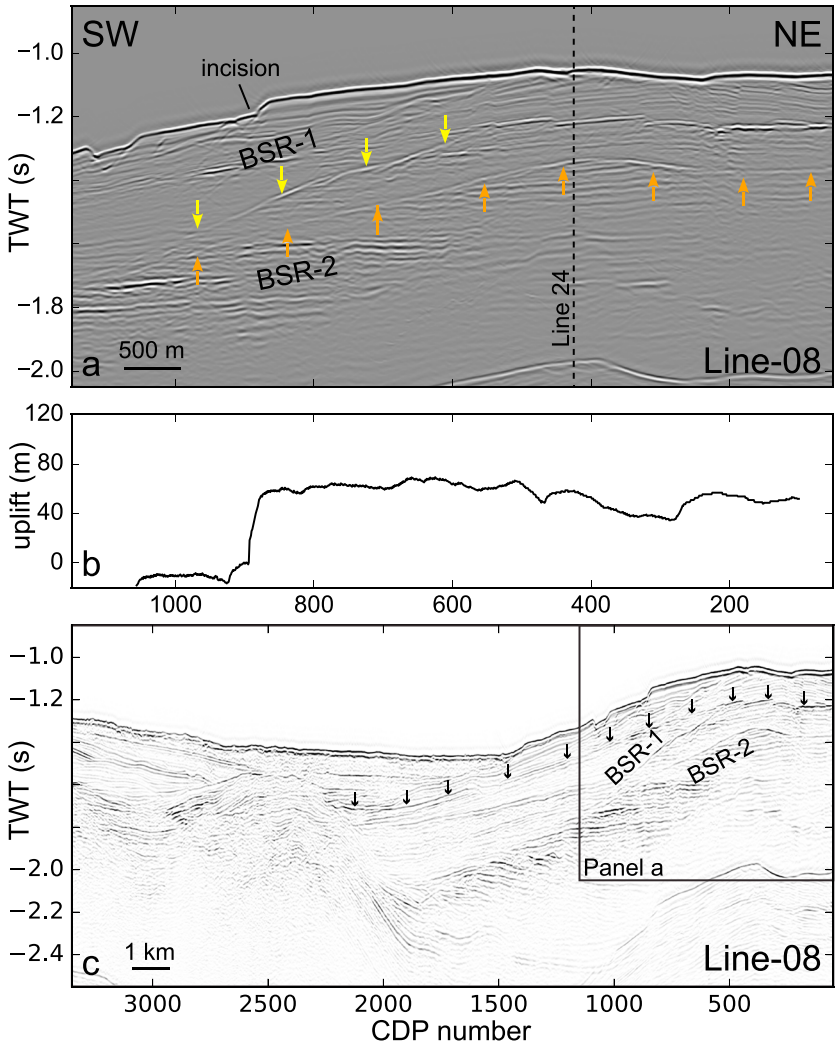

Figure 3. (a) Seismic line 8. The dashed vertical line marks crossing with line 24 (Figure 2). (b) Uplift along line 8 calculated, assuming BSR-2 is paleo-BSR. (c) Regional display of line 8. The arrows mark a reflection that is buckling upward beneath the ridge, compatible with uplift.

were converted to heat flux using thermal conductivity measurements at six stations (Figure S2). The average thermal conductivity from these stations was used for the other stations. We roughly estimated error margins for thermal gradients as 1% and for thermal conductivity as 5%. These values are well below the standard deviation from averaging over several stations that we use later (further details in Figures S1 and S2 and Table S1 in the supporting information).

Thermal gradient and heat flux were also constrained from the depth of BSRs. Bottom-water temperatures were extracted from historic conductivity-temperature-depth readings from a region within ~100–150 km of our study area (Chiswell, 2005; Mountjoy et al., 2014). Temperature at the BSR was obtained from the methane hydrate phase boundary using the Colorado School of Mine's HYDOFF code (Sloan & Koh, 2007), corrected for seawater (Dickens & Quinby-Hunt, 1994) and assuming hydrostatic pressure. The assumption of methane for hydrate formation is based on geochemical analyses of a number of seafloor cores from the Hikurangi Margin (e.g., Coffin et al., 2014; Greinert et al., 2010). For time-to-depth conversion, seismic velocity was assumed to be 1,500 m/s in the water column and 1,700 m/s between seafloor and BSR based on ocean-bottom seismometer data (Wild, 2016). We used 1,800 m/s for low-end estimates of BSR heat flux. The upper bound of BSR heat flux was estimated using a velocity of 1,600 m/s, lithostatic pressure, and freshwater. Sediment density for lithostatic pressure was calculated using Gardner's equation (Gardner et al., 1974), which yielded higher densities and thus was more appropriate for an upper bound of heat flux than the

alternative Hamilton equation (Hamilton, 1978). We did not perform any bathymetry corrections because our study relies only on comparison of seafloor and BSR heat flux, which should be affected similarly by topography. The average bulk thermal conductivity from the seafloor heat probes was used to convert thermal gradients to heat flux.

2.2. Analysis of Double-BSRs

We try to distinguish between uplift and admixing of sII-hydrate forming gases as possible causes for BSR-2 by (1) constraining the amount of uplift if BSR-2 is a paleo-BSR and (2) comparing predicted pressure-temperature conditions at BSR-2 to phase boundaries of hydrates containing varying fractions of sII-forming propane.

Uplift was calculated based on the assumption that the preuplift two-way travel time (TWT) of the paleo-BSR, BSR-2, beneath the seafloor as a function of water depth (in TWT) was identical to the TWT of the current BSR-1. We determined TWT to seafloor t_s and BSR-1 t_1 and the travel time difference $\Delta t = t_1 - t_s$. We sorted the resulting array of $\Delta t(t_s)$ according to t_s and extracted a fifth-order polynomial best fit function (Table S2 and Figure 2d). We then determined TWT from seafloor to BSR-2 and used the best fit function of $\Delta t(t_s)$ to constrain preuplift TWT of the paleo-seafloor. The use of observed $\Delta t(t_s)$ decreases uncertainties. We do not, for example, require any information on gas or pore water composition. Implicitly, we assume laterally constant subseafloor thermal gradients.

To test whether admixing of sII-hydrate forming gases may lead to a second BGHS at BSR-2, we predicted pressure-temperature conditions at the depth of BSR-2 using a subseafloor velocity of 1,700 m/s to convert TWT to depth, water temperatures from our calculations of BSR heat flow, and temperature gradients from the seafloor heat probes. Depth was converted to hydrostatic pressure in seawater. Pressure-temperature values were compared to phase diagrams of methane-propane mixes in seawater for fractions of propane up to 0.3, beyond which the phase boundary does not change noticeably (hydrate from pure propane dissociates to the liquid phase at these pressures; Makogon, 2003). We assumed only propane as sII-hydrate forming gas because of a lack of information on gas composition, and thus, these calculations are qualitative.

3. Results

3.1. Heat Flux

Seafloor thermal gradient and heat flux are shown in Figures 2b and 2c. The average thermal conductivity is 1.2 ± 0.1 W K^{-1} m^{-1}. Thermal gradients and heat flux from BSRs for our baseline case are 0.021 K m^{-1} and 0.025 W m^{-2}, respectively. Upper and lower bounds for thermal gradients are 0.032 K m^{-1} and 0.020 K m^{-1}, corresponding to 0.038 W m^{-2} and 0.024 W m^{-2} for heat flux. These compare well with seafloor measurements above BSR-1 (Stations 13 and higher) with thermal gradients of 0.022 ± 0.004 K m^{-1} and heat flux values of 0.027 ± 0.005 W m^{-2}. These error margins are standard deviations from the mean of measurements at several stations that far exceed estimated error margins for measurements at individual stations and thus form the basis for our further analysis.

The thermal gradient from the seafloor heat probes increases significantly over a distance of ~1 km across the area where BSR-1 approaches the seafloor, the updip limit of the BGHS, between Stations 13 and 6. The thermal gradient remains elevated for the remainder of the transect >2 km further to the northwest. Stations 1–6 measured a mean thermal gradient of 0.070 ± 0.012 K m^{-1} and heat flux of 0.086 ± 0.015 W m^{-2}.

3.2. Analysis of Double-BSRs: Uplift

BSR-2 is present along Line 24 over a range of water depths (~650–800 m) until it disappears toward the southeast (Figure 2a). Using the $\Delta t(t_s)$ relation in Figure 2d, predicted uplift along Line 24 is relatively constant with an average of 73 m (Figure 2e). A notch around CDP 8750 correlates with a dip in the seafloor and may be an artifact from erosion during or after uplift. Error margins are largely determined by uncertainties in the $\Delta t(t_s)$ function. The RMS error between calculated $\Delta t(t_s)$ and observations is 0.007 s. However, our calculations are sensitive to incisions on the seafloor that may reflect small-scale erosion. If cooling resulting from seafloor erosion has not reached BSR-2, seafloor incisions lead to an underestimate of uplift. The notches on the seafloor are around ±0.02 s, which we assume as error margin for $\Delta t(t_s)$, corresponding to ±15 m.

In Line 08, both BSRs converge toward the southwest (Figure 3a) at the level of BSR-1 (compared to Line 24). BSR-2 continues toward the northeast beyond Line 8. Uplift along Line 8 was calculated using the $\Delta t(t_s)$ function from Line 24 because the relatively small range of water depths did not allow determining a function from Line 8. Uplift is nearly constant with an average of 56 ± 15 m over much of the line until it decreases toward the point of BSR convergence (Figure 3b). The sharp edge toward the southwest is exaggerated because it coincides with an incision in the seafloor that may mark an erosional scar. We focus our discussion on Line 24 because of the lack of a $\Delta t(t_s)$ function from Line 8 and because Line 8 was acquired in a direction parallel to the slope, which may introduce artifacts (Yilmaz, 2008).

3.3. Analysis of Double-BSRs: Thermogenic Gas

We predicted pressure-temperature conditions at BSR-2 at CDPs 8,600 and 8,900 along Line 24, assuming thermal gradients of 0.022 K m^{-1} and 0.070 K m^{-1} and compared them to phase diagrams of hydrates formed from methane-propane-mixed gases in seawater. For the lower thermal gradient measured at the seafloor above BSR-1, only ~0.5% of propane are required to match the phase boundary. Propane fractions need to be significantly higher if assuming the higher thermal gradients, exceeding the stability of hydrates from methane-propane mixes at CDP 8,600.

4. Discussion

4.1. Fluid Advection

The thermal gradient above BSR-1 is similar to values reported in previous studies (Henrys et al., 2003; Pecher et al., 2010; Townend, 1997). Hence, thermal gradients landward of the updip limit of the BGHS are anomalously high. We propose that this anomaly is caused by advective heat flux associated with fluid expulsion. Advective heat flux leads to concave thermal profiles. Fluid flux rates required to increase the thermal gradient at the seafloor from 0.022 K m^{-1} to 0.070 K m^{-1} were estimated based on a 1-D analytical solution (Bredehoeft & Papadopulos, 1965). This solution assumes fixed temperatures at base and top of a layer and calculates the temperature-depth profile through the layer as a function of Darcy velocities. The base of the model is considered to be the depth at which advection starts contributing to heat flow. This method investigates the thermal response from a prescribed flux of fluids, irrespective of any hydraulic processes.

Thermal properties are assumed to be constant with depth. In order to accommodate a decrease of porosity, resulting in an increase of thermal conductivity with depth, we mimicked a two-layer case: thermal conductivity was kept constant from the seafloor to the base of a slope basin z_{bas} = 2,000 mbsf (m beneath the seafloor) using the mean value for conductivity from the heat probe measurements, k_{bas} = 1.2 W m^{-1} K^{-1}. The basin is underlain by an accretionary wedge with lower porosity. Bulk thermal conductivity in the accretionary wedge k_{accr} was calculated from porosity ϕ using the geometric average, $k_{accr} = k_f^{\phi} k_g^{1-\phi}$ (e.g., Villinger et al., 1994). Porosity was assumed to be 0.2 down to the depth of the subduction interface z_{sub} = 7,000 mbsf. These values are based on model kilometer 42.5 in Ellis et al. (2015). Assuming grain and pore fluid conductivities k_g = 0.6 W m^{-1} K^{-1} and k_f = 2.8 W m^{-1} K^{-1}, respectively, k_{accr} = 2.1 W m^{-1} K^{-1}. The specific heat capacity of the pore fluid, needed to model advective heat transport along with pore fluids, was set to that of water, c_f = 4, 180 J kg^{-1} K^{-1}. While not accounting for compaction within the basin, we consider this simplification a practically feasible approach for using seafloor geothermal gradients to estimate advective heat flux based on the analytical solution by Bredehoeft and Papadopulos (1965). Equations are summarized in Text S1 in the supporting information and input parameters in Table S3 (Minshull & White, 1989; Pecher et al., 2010; Xu & Ruppel, 1999).

Temperature at the seafloor was fixed at 8°C based on input values for BSR heat flux. We simulated two scenarios, a depth for the source of advective heat flux at z_{accr} = 3,500 mbsf (in the accretionary prism) and at the subduction interface z_{sub} = 7,000 mbsf. Temperatures at these depth levels were obtained from the conductive heat equation, k_{bas}, k_{accr}, and seafloor heat flux of 0.025 W m^{-2}. Temperatures were 52°C and 112°C at z_{accr} and z_{sub}, respectively (Figure 4a). The latter is within the range predicted by Ellis et al. (2015) at the subduction interface (80–150°C).

We used the assumption that total heat flux (conductive and advective) across the interface between both layers is constant to determine the temperature T_{bas} at z_{bas} iteratively. Darcy velocities of 6 and 10 mm/yr

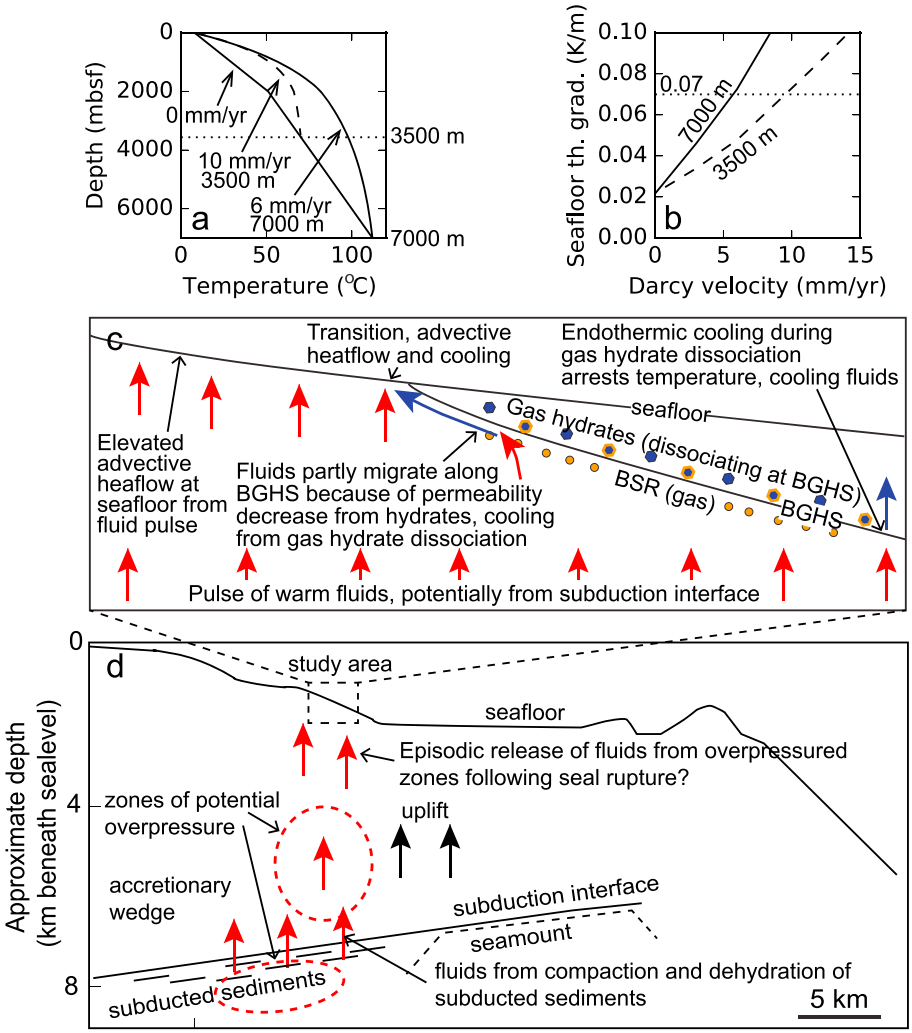

Figure 4. (a) Temperature as function of depth for two-layer case of thermal conductivity without advective heat flux (0 mm/yr) and with advective heat flux such that the observed thermal gradient of 0.07 K/m at the seafloor is reached. Source of advective flux at 3,500 and 7,000 mbsf. (b) Thermal gradient at the seafloor as a function of Darcy velocities. Source of advective flux at 3,500 and 7,000 mbsf. (c) Conceptual mechanisms leading to observed heat flux anomaly. (d) Conceptual model of seamount subduction leading to advective fluid pulse and uplift. Fluid-flow-related processes after Ellis et al. (2015), structural features after Bell et al. (2010, 2014).

are required if advective heat flux starts at 7,000 and 3,500 mbsf, respectively. The former value is similar to ~5 mm/yr predicted for the Porangahau Ridge further to the south where BSR updoming marks a pronounced heat flux anomaly (Pecher et al., 2010). Because of the many simplifications, our results are only indicative to demonstrate that these predicted rates are realistic for subduction zones (e.g., Kukowski & Pecher, 1999). The depth at which fluid expulsion contributes to heat flux may be shallower if focusing of fluid expulsion is occurring. The lack of suitable data, such as 3-D seismic images, does not allow us to more accurately pinpoint the source of fluid expulsion.

Our transect is located above a high reflectivity zone identified in deep-penetration seismic reflection data (HRZ-2 in Bell et al., 2010) (Figure 1). These high reflectivity zones are thought to consist of 2–4 km thick underthrust sediments and material from the overriding plate with high fluid and/or varying sand content in an area where the décollement is being forced upward ahead of subduction of seamounts (Bell et al., 2010). We speculate these thick sediment packages may be the source of fluid advection. Modeling of seamount subduction by Ellis et al. (2015) along Line 05CM-04 predicts significant overpressure between ~3,500 and 7,000 mbsf (note, ~1,000 m of water column need to be added for comparison to our results).

Depending largely on permeability, their models predict high pore pressure in the accretionary wedge at ~3,500 mbsf and the subduction interface at ~7,000 mbsf. We suggest that fluids originate from these overpressured regions.

4.2. Transient Fluid Pulse

The thermal anomaly is limited to the region above the updip limit of the BGHS. It is possible that the edge of the advective heat flux anomaly simply coincides with this location. However, we propose that the absence of anomalously high-temperature gradients above gas hydrate bearing sediments is best explained by latent heat depressing temperatures during hydrate dissociation. In that case, the thermal system has not reached steady state, suggesting that advective heat flux is transient. Studies investigating the response of gas hydrates to uplift indicate that such endothermal cooling can arrest temperatures at the phase boundary for thousands of years (Goto et al., 2016). We suggest that it may also take a considerable time for gas hydrate systems to adjust to an increase in temperature. In addition, the intensity of any fluid pulses, that is, fluid velocities, may be dampened by a permeability decrease from hydrates. The transition zone from low-to-high thermal gradients may be caused by mixing of warm, upward migrating fluids and fluids that are partly deflected at the BGHS because of a decrease of permeability in gas-hydrate bearing sediments (e.g., Kang et al., 2016) and cooled by dissociating gas hydrates while migrating along the BGHS.

We can only speculate as to the processes that may control the transient nature of fluid release. It is widely recognized that earthquakes lead to significant changes in the hydrologic regime affecting many near-surface processes such as geyser, mud volcanoes, and springs (e.g., Wang & Manga, 2010, and references therein). Fluid-flow pulses associated with earthquakes have recently also been confirmed from temperature fluctuations in boreholes (Fulton & Brodsky, 2016). Permeability changes in particular are expected to influence fluid flow. An increase of *Vp/Vs* near the subduction interface at ~30 km depth over a 50 day period following the 1995 M_w 8.0 Antofagasta earthquake (Husen & Kissling, 2002) may be linked to a pore pressure pulse following coseismic rupture of a seal separating overpressured subducted sediments from the overriding plate (Koerner et al., 2004). We speculate that similar seal rupture may occur above overpressured zones in our study area, for example, associated with earthquakes or slow-slip events (Wallace & Beavan, 2010), resulting in fluid pulses.

4.3. Double-BSR

Our study area is part of New Zealand's East Coast Basin, which contains several potential mid-Cretaceous to Late Paleocene source rocks, in particular the Waipawa Formation (e.g., Hollis & Manzano-Kareah, 2005). A thermogenic origin of gas is therefore a possibility. Comparison between predicted pressures and temperatures at CDP 8,600 to the phase boundary of hydrates from methane and propane gas mixes makes it unlikely that BSR-2 formed from sII hydrates under the thermal regime of elevated, advective heat flux, for example, by thermogenic gas that is being transported along with a fluid pulse (Figure 2f). However, BSR-2 may be caused by sII hydrates at the phase boundary for the long-term, conductive thermal field (Figure 2f). In this scenario, sII hydrates must have dissociated sufficiently to not depress temperatures at BSR-2 while still causing sufficient gas to be trapped at BSR-2 to form a continuous reflection. Given the strong sensitivity of hydrate stability to sII-hydrate forming gas, it also needs to be explained why BSR-2 is laterally smooth—small changes in propane concentration should lead to significant fluctuations of BSR-2 depth.

We do not rule out sII-hydrate forming thermogenic gas as cause of BSR-2—such gas fractionation associated with gas hydrate formation in marine sediments is still poorly understood. However, we favor uplift as the cause of BSR-2 based on our hydrate-stability models. The lack of a trend for the predicted uplift rate over a range of water depths is not trivial. Because of the nonlinearity of the pressure-temperature relation of the gas hydrate phase boundary, the depth interval between the two BSRs for a given rate of uplift decreases with increasing water depth. The gap between both BSRs is 120 m (for a velocity of 1,700 m/s) near the upper termination of BSR-1 at 660 m water depth and 70 m near the lower termination of BSR-2 at 810 m water depth.

The region with double-BSRs is located above a seafloor ridge (Figure 1b). While we do not have any suitable data for imaging deep structural features, the stratigraphy beneath the ridge shows subparallel upward buckling of layers, supporting uplift relative to the adjacent basin (Figure 3c).

BSR-2 is a distinct reflection because net depressurization from uplift probably only started ~7,000 years ago. Any depressurization from uplift before then was likely counteracted by an increase in pressure from rapid eustatic sea level rise of ~100 m within ~8,000 years (~12.5 mm/yr). Sea level rise plateaued ~7,000 years ago (e.g., Lambeck et al., 2014). If we assume that BSR-2 marks the paleo-BSR at that time, our predicted uplift of 70 m results in an uplift rate of 10 mm/yr.

This value is high compared to long-term Quaternary uplift rates observed onshore of at most 2–4 mm/yr (Nicol et al., 2017). A possible increase in bottom-water temperatures over the past 7,000 years may have contributed to an upward movement of the BGHS. Its contribution, however, would need to be sufficiently small that paleo- and recent levels of the BGHS are not discernible beyond the point of BSR convergence along Line 8.

We speculate that seamount subduction causes both high rates of uplift and advective heat flux (Figure 4d). The peak of a magnetic anomaly marking a buried seamount (Bell et al., 2014) (Figure 1d) lies to the east of our study area, indicating that the double-BSRs are situated near the leading flank of this seamount where significant uplift would be expected (Ding & Lin, 2016). Bell et al. (2014) modeled slip along the rupture zone of the 1947 Offshore Poverty Bay earthquake on the eastern flank of this seamount using tsunami runup heights and seismic waveforms. Predicted seafloor uplift for their preferred model was 0.9–1.3 m with estimated recurrence rates of 70–90 years (supporting information in Bell et al., 2014). This is equivalent to uplift rates of 10–19 mm/yr, similar to our predicted uplift rate of ~10 mm/yr. Seamount topography could explain a decrease of uplift from north to south along Line 8 as suggested by BSR convergence.

4.4. Effects on Gas Hydrates

Assuming fluid pulses are episodic, we predict repeated gas hydrate dissociation and formation at the BGHS. Resulting pore pressure fluctuations could cause weakening of sediments. This process is similar to the proposed mechanism of gas hydrate "frost heave" from repeated hydrate dissociation because of bottom-water temperature fluctuation proposed for seafloor erosion on Rock Garden further south (Crutchley et al., 2010; Ellis et al., 2010; Pecher et al., 2005). We speculate that fluid pulses and their effect on hydrate-bearing sediments may also play a role in "creeping" (slow deformation) of the Tuaheni Landslide Complex ~30 km to the southwest of our study area, where slow deformation seems linked to gas hydrates (Mountjoy et al., 2014).

5. Conclusions

We observe a significant increase of the thermal gradient on the seafloor across the updip limit of the BGHS. This increase is best explained by a fluid pulse leading to advective heat flux, which is buffered by endothermic cooling in the gas hydrate stability field. The fluid pulse may originate from fluid expulsion deep in the subduction zone. Double-BSRs in the study are likely to be linked to uplift. We propose that both uplift and fluid expulsion are caused by subduction of a seamount on the Pacific Plate. Our findings add to the increasing evidence for the transient nature of fluid expulsion in subduction zones.

Acknowledgments
We thank the captains and crews of the R/V *Sonne* and R/V *Tangaroa* for their excellent work during voyages SO-247 and TAN1114. This study was supported by the New Zealand Ministry for Business Innovation and Employment contract C05X0908, by public good research funding from the Government of New Zealand to GNS Science, and by the U.S. Department of Energy grant DE-FE0026163. Voyage SO-247 was funded by the German Bundesministerium für Bildung und Forschung under BMBF grant 03G0247A/B SO 247–SLAMZ and R/V *Tangaroa* voyage TAN1114 by Land Information New Zealand's OS2020 program. Seafloor heat flux data are available from the data publisher PANGAEA (https://pangaea.de/), seismic data through New Zealand Petroleum and Minerals (https://www.nzpam.govt.nz/maps-geoscience/), and codes from the corresponding author. We thank A. Tréhu and an anonymous reviewer for their thoughtful comments which significantly aided in improving the manuscript.

References

Bangs, N. L., Musgrave, R. J., & Tréhu, A. M. (2005). Upward shifts in the southern hydrate ridge gas hydrate stability zone following postglacial warming, offshore Oregon. *Journal of Geophysical Research*, *110*, B03102. https://doi.org/10.1029/2004JB003293

Barnes, P., & TAN 1114 scientific party (2011). NIWA voyage report TAN1114, Rep., 45 pp, National Institute of Water and Atmospheric Research.

Bell, R., Holden, C., Power, W., Wang, X., & Downers, G. (2014). Hikurangi margin tsunami earthquake generated by slow seismic rupture over a subducted seamount. *Earth and Planetary Science Letters*, *307*, 1–9. https://doi.org/10.1016/j.epsl.2014.04.0050012-821X.

Bell, R. F., Sutherland, R., Barker, D. H. N., Henrys, S., Bannister, S., Wallace, L., & Beavan, J. (2010). Seismic reflection character of the Hikurangi subduction interface, New Zealand, in the region of repeated Gisborne slow slip events. *Geophysical Journal International*, *180*(1), 34–48. https://doi.org/10.1111/j.1365-246X.2009.04401.x

Bredehoeft, J. D., & Papadopulos, I. S. (1965). Rates of vertical groundwater movement estimated from the Earth's thermal profile. *Water Resources Research*, *1*(2), 325–328. https://doi.org/10.1029/WR001i002p00325

Chiswell, S. (2005). Mean and variability in the Wairarapa and Hikurangi eddies. *New Zealand Journal of Marine and Freshwater Research*, *39*(1), 121–134. https://doi.org/10.1080/00288330.2005.9517295

Coffin, R. B., Hamdan, L. J., Smith, J. P., Rose, P. S., Plummer, R. E., Yoza, B., … Montgomery, M. T. (2014). Contribution of vertical methane flux to shallow sediment carbon pools across Porangahau ridge, New Zealand. *Energies*, *7*(8), 5332–5356. https://doi.org/10.3390/en7085332

Crutchley, G. J., Geiger, S., Pecher, I. A., Gorman, A. R., Zhu, H., & Henrys, S. A. (2010). The potential influence of shallow gas and gas hydrates on seafloor erosion of rock garden, an uplifted ridge offshore of New Zealand. *Geo-Marine Letters*, *30*(3-4), 283–303. https://doi.org/10.1007/s00367-010-0186-y

Crutchley, G. J., Klaeschen, D., Planert, L., Bialas, J., Berndt, C., Papenberg, C., … Brueckmann, W. (2014). The impact of fluid advection on gas hydrate stability: Investigations at sites of methane seepage offshore Costa Rica. *Earth and Planetary Science Letters*, *401*, 95–109. https://doi.org/10.1016/j.epsl.2014.05.045

Davy, B., Pecher, I. A., Wood, R., Carter, L., & Gohl, K. (2010). Gas escape features off New Zealand—Evidence for a massive release of methane from hydrates. *Geophysical Research Letters*, *37*, L21309. https://doi.org/10.1029/2010GL045184

Dickens, G. R., & Quinby-Hunt, M. S. (1994). Methane hydrate stability in seawater. *Geophysical Research Letters*, *21*(19), 2115–2118. https://doi.org/10.1029/94GL01858

Ding, M., & Lin, J. (2016). Deformation and faulting of subduction overriding plate caused by a subducted seamount. *Geophysical Research Letters*, *43*, 8936–8944. https://doi.org/10.1002/2016GL069785

Ellis, S., Fagereng, A., Barker, D., Henrys, S., Saffer, D., Wallace, L., … Harris, R. (2015). Fluid budgets along the northern Hikurangi subduction margin, New Zealand: The effect of a subducting seamount on fluid pressure. *Geophysical Journal International*, *202*, 277–297. https://doi.org/10.1093/gji/ggv127

Ellis, S., Pecher, I. A., Kukowski, N., Xu, W., Greinert, J., & Henrys, S. (2010). Testing proposed mechanisms for seafloor weakening at the top of gas hydrate stability, rock garden, New Zealand. *Marine Geology*, *272*(1-4), 127–140. https://doi.org/10.1016/j.margeo.2009.10.008

Foucher, J.-P., Nouzé, H., & Henry, P. (2002). Observation and tentative interpretation of a double BSR on the Nankai slope. *Marine Geology*, *187*(1-2), 161–175. https://doi.org/10.1016/S0025-3227(02)00264-5

Fulton, P., & Brodsky, E. (2016). In situ observations of earthquake-driven fluid pulses within the Japan Trench plate boundary fault zone. *Geology*, *44*(10), 851–854. https://doi.org/10.1130/G38034.1

Gardner, G. H. F., Garnder, L. W., & Gregory, A. R. (1974). Formation velocity and density—The diagnostic basics for stratigraphic traps. *Geophysics*, *39*(6), 770–780. https://doi.org/10.1190/1.1440465

Goto, S., Matsubayashi, O., & Nagakubo, S. (2016). Simulation of gas hydrate dissociation caused by repeated tectonic uplift events. *Journal of Geophysical Research : Solid Earth*, *121*, 3200–3219. https://doi.org/10.1002/2015JB012711

Greinert, J., Lewis, K. B., Bialas, J., Pecher, I. A., Rowden, A., Bowden, D. A., … Linke, P. (2010). Methane seepage along the Hikurangi margin, New Zealand: Overview of studies in 2006 and 2007 and new evidence from visual, bathymetric and hydroacoustic investigations. *Marine Geology*, *272*(1-4), 6–25. https://doi.org/10.1016/j.margeo.2010.01.017

Hamilton, E. L. (1978). Sound velocity-density relations in sea-floor sediments and rocks. *The Journal of the Acoustical Society of America*, *43*, 366–377.

Henrys, S. A., Ellis, S., & Uruski, C. (2003). Conductive heat flow variations from bottom-simulating reflectors on the Hikurangi margin, New Zealand. *Geophysical Research Letters*, *30*(2), 1065. https://doi.org/10.1029/2002GL015772

Hollis, C. J., & Manzano-Kareah, K. (2005). Source rock potential of the East Coast Basin Rep. PR3179, 158 pp, New Zealand Petroleum and Minerals.

Huhn, K. (2016). Cruise report/Fahrtbericht SO-247 SlamZRep., 116 pp, University of Bremen, Bremen.

Husen, S., & Kissling, E. (2002). Postseismic fluid flow after the large subduction earthquake of Antofagasta, Chile. *Geology*, *29*(9), 847–850.

Hyndman, R. D., Davis, E. E., & Wright, J. A. (1979). The measurements of marine geothermal heat flow by a multipenetration probe with digital acoustic telemetry and in situ conductivity. *Marine Geophysical Researches*, *4*, 181–205.

Kang, D. H., Yuin, T. S., Kim, K. Y., & Jang, J. (2016). Effect of hydrate nucleation mechanisms and capillarity on permeability reduction in granular media. *Geophysical Research Letters*, *43*, 9018–9025. https://doi.org/10.1002/2016GL07051.

Koerner, A., Kissling, E., & Miller, S. (2004). A model of deep crustal fluid flow following the Mw = 8.0 Antofagasta, Chile, earthquake. *Journal of Geophysical Research*, *109*, B06307. https://doi.org/10.1029/2003JB002816

Kukowski, N., & Pecher, I. A. (1999). Thermo-hydraulic modelling of the accretionary complex off Peru at 12°S. *Journal of Geodynamics*, *27*(3), 373–402. https://doi.org/10.1016/S0264-3707(98)00009-X

Kvenvolden, K. A. (1993). Gas hydrates—Geologic perspective and global change. *Reviews of Geophysics*, *31*(2), 173–187. https://doi.org/10.1029/93RG00268

Lambeck, K., Rouby, H., Purcell, A., Sun, Y., & Sambridge, M. (2014). Sea level and global ice volumes from the Last Glacial Maximum to the Holocene. *Proceedings of the National Academy of Sciences of the United States of America*, *111*(43), 15,296–15,303. https://doi.org/10.1073/pnas.1411762111

Lister, C. R. B. (1979). The pulse-probe method of conductivity measurements. *Geophysical Journal of the Royal Astronomical Society*, *57*(2), 451–461. https://doi.org/10.1111/j.1365-246X.1979.tb04788.x

Makogon, Y. F. (2003). Liquid propane + water phase equilibria at hydrate conditions. *Journal of Chemical & Engineering Data*, *48*(2), 347–350. https://doi.org/10.1021/je020143w

Minshull, T. A., & White, R. (1989). Sediment composition and fluid migration in the Makran accretionary prism. *Journal of Geophysical Research*, *94*(B6), 7387–7402. https://doi.org/10.1029/JB094iB06p07387

Mountjoy, J. J., Pecher, I., Henrys, S., Crutchley, G., Barnes, P. M., & Plaza-Faverola, A. (2014). Shallow methane hydrate system controls ongoing, downslope sediment transport in a low-velocity active submarine landslide complex, Hikurangi margin, New Zealand. *Geochemistry, Geophysics, Geosystems*, *15*, 4137–4156. https://doi.org/10.1002/2014GC005379

Nicol, A., Seebeck, H., & Wallace, L. (2017). Quaternary tectonics of New Zealand. In J. Shulmeister (Ed.), *Landscape and Quaternary environmental change in New Zealand* (pp. 1–34). Amsterdam: Atlantis Press.

Paganoni, M., Cartwright, J. A., Foschi, M., Shipp, R. C., & Van Rensbergen, P. (2016). Structure II gas hydrates found below the bottom simulating reflector. *Geophysical Research Letters*, *43*, 5696–5706. https://doi.org/10.1002/2016GL069452

Pecher, I. A., Crutchley, G., Mountjoy, J., Gorman, A. R., Fraser, D., & Henrys, S. A. (2014). Double BSRs on the Hikurangi margin, New Zealand—Possible implications for gas hydrate stability and composition, in Proc. 8th International Conference on Gas Hydrates, edited, p. 6 pp., Beijing.

Pecher, I. A., Henrys, S. A., Ellis, S., Chiswell, S. M., & Kukowski, N. (2005). Erosion of the seafloor at the top of the gas hydrate stability zone on the Hikurangi margin, New Zealand. *Geophysical Research Letters*, *32*, L24603. https://doi.org/10.1029/2005GL024687

Pecher, I. A., Henrys, S. A., Kukowski, N., Crutchley, G. J., Gorman, A. R., Wood, W. T., … CHARMNZ Working Group (2010). Focussing of fluid expulsion on the Hikurangi margin, New Zealand, based on evidence for free gas in the regional gas hydrate stability zone. *Marine Geology*, *272*, 99–113.

Phrampus, B. J., & Hornbach, M. J. (2012). Recent changes to the Gulf Stream causing widespread gas hydrate dissociation. *Nature*, *490*(7421), 527–530. https://doi.org/10.1038/nature11528

Saffer, D. M., & Bekins, B. A. (1998). Episodic fluid flow in the Nankai accretionary complex: Timescale, geochemistry, flow rates, and fluid budget. *Journal of Geophysical Research*, *103*(B12), 30,351–30,370. https://doi.org/10.1029/98JB01983

Saffer, D. M., & Bekins, B. A. (1999). Fluid budgets at convergent plate margins: Implications for the extent and duration of fault-zone dilation. *Geology*, *27*(12), 1095–1098. https://doi.org/10.1130/0091-7613(1999)027%3C1095:FBACPM%3E2.3.CO;2

Sloan, E. D., & Koh, C. A. (2007). *Clathrate hydrates of natural gases* (3rd ed.p. 721). New York: Marcel Bekker.
Sutherland, R. (1996). Magnetic anomalies in the New Zealand region, 1:4,000,000, Institute of Geological & Nuclear Sciences, Lower Hutt.
Townend, J. (1997). Estimates of conductive heat flow through bottom-simulating reflectors on the Hikurangi margin and southwest Fiordland, New Zealand. *Marine Geology*, *141*(1-4), 209–220. https://doi.org/10.1016/S0025-3227(97)00073-X
Tréhu, A. M., Stakes, D. S., Bartlett, C. D., Chevallier, J., Duncan, R. A., Goffredi, S. K., … Salamy, K. A. (2003). Seismic and seafloor evidence for free gas, gas hydrates, and fluid seeps on the transform margin offshore Cape Mendocino. *Journal of Geophysical Research*, *108*(B5), 2263. https://doi.org/10.1029/2001JB001679
Villinger, H. W., Langseth, M. G., Göschel-Becker, H. M., & Fisher, A. T. (1994). Estimating in-situ thermal conductivity from log data. In M. J. Moul, et al. (Eds.), *Proc. ODP, Sci. Results* (pp. 545–552). College Station, TX: Ocean Drilling Program.
Villinger, H. W., Tréhu, A. M., & Grevemeyer, I. (2010). Seafloor marine heat flux measurements and estimation of heat flux from seismic observations of bottom simulating reflectors. In M. Riedel, E. C. Willoughby, & S. Chopra (Eds.), *Geophysical characterization of gas hydrates* (pp. 279–300). Tulsa, OK: Society of Exploration Geophysicists.
Wallace, L. M., & Beavan, J. (2010). Diverse slow slip behavior at the Hikurangi subduction margin, New Zealand. *Journal of Geophysical Research*, *114*, B12402. https://doi.org/10.1029/2010JB007717
Wang, C., & Manga, M. (2010). Hydrologic responses to earthquakes and a general metric. *Geofluids*, *10*, 206–216. https://doi.org/10.1111/j.1468-8123.2009.00270.x
Wild, J. J. (2016). *Seismic velocities beneath creeping gas hydrates slides—Analysis of ocean bottom seismometer data in the Tuaheni Landslide Complex on the Hikurangi Margin*, New Zealand, University of Auckland, Auckland.
Xu, W., & Ruppel, C. D. (1999). Predicting the occurrence, distribution, and evolution of methane gas hydrate in porous marine sediments. *Journal of Geophysical Research*, *104*(B3), 5081–5095. https://doi.org/10.1029/1998JB900092
Yilmaz, Ö. (2008). *Seismic data analysis* (3rd ed.). Tulsa, OK: Society of Exploration Geophysicists.
Zander, T., Haeckel, M., Berndt, C., Chi, W.-C., Klaucke, I., Bialas, J., … Atgin, O. (2017). On the origin of multiple BSRs in the Danube deep-sea fan, Black Sea. *Earth and Planetary Science Letters*, *462*, 15–25. https://doi.org/10.1016/j.epsl.2017.01.006